scientific reports

Check for updates

OPEN

Complex forming properties of cannabinoid acids in a green solvent and bioassays focused on gastric disease caused by *Helicobacter pylori* infection

Magdalena Woźniczka[1]✉, Marek Pająk[1], Manas Sutradhar[2,3], Mirosława Świątek[1], Beata Pasternak[4], Adília Januário Charmier[2], Ewelina Namiecińska[5] & Weronika Gonciarz[6]✉

The main objective of the present study was to determine the protolytic and coordination properties of two bioactive cannabinoid acids (cannabidiolic acid and cannabigerolic acid) in ethyl alcohol-water mixture (50/50, v/v). The complexation properties of these acids with copper(II) and zinc(II) ions were determined by potentiometric and ESI–MS methods. UV–Vis absorption spectra for the copper(II) systems confirmed the speciation models with one type of complex indicating coordination with completely deprotonated dinegative ligand molecule. The occurrence of precipitation at lower pH values limited the ability to determine complexes under these conditions. The research also aimed to identify potential biological and medicinal applications of cannabinoid acids and their complexes with zinc(II). The ability of these compounds to influence the growth of human Hs68 skin fibroblasts and AGS gastric adenocarcinoma cells was investigated. Furthermore, these structures were tested against *Helicobacter pylori* strains, one of the factors promoting gastric cancer development. At concentrations that were not-toxic to healthy cells (after dilution of the solutions, the composition of the ethanol/water mixture was approximately 1/99, v/v), the ligands exhibited bacterial inhibitory activity and cytotoxic properties against AGS cancer cells. Zinc(II) complexes, on the other hand, being biologically safe for all cells, had strong antibacterial properties, both inhibitory and bactericidal.

Keywords Cannabinoid acids, Copper(II) complex, Zinc(II) complex, Anticancer activity, *Helicobacter pylori*, Stability constant

Naturally occurring compounds known as plant cannabinoids or phytocannabinoids, responsible for the physiological effects of cannabis, have been used medicinally for thousands of years. The main non-psychoactive ingredient is cannabidiol (CBD) which induces various pharmacological effects by interacting with an endogenous lipid-signaling network known as the endocannabinoid system[1,2]. CBD has been shown to regulate the intracellular calcium action. Its therapeutic potential has been linked to antiemetic, anticonvulsant, anti-inflammatory and antipsychotic properties, used in a wide range of conditions, including multiple sclerosis, schizophrenia, bipolar mania, social anxiety disorder, insomnia, Huntington's disease, diabetes, cancer and epilepsy[1,3].

In most cannabis plant varieties, CBD is produced by the gradual non-enzymatic decarboxylation of a compound called cannabidiolic acid (CBDA, Fig. 1), and this process is accelerated by light or heat. In

[1]Department of Physical and Biocoordination Chemistry, Faculty of Pharmacy, Medical University of Lodz, Muszyńskiego 1, 90-151 Lodz, Poland. [2]Faculdade de Engenharia, Universidade Lusófona — Centro Universitário de Lisboa, Campo Grande 376, 1749-024 Lisboa, Portugal. [3]Centro de Química Estrutural, Instituto Superior Técnico, Universidade de Lisboa, Av. Rovisco Pais, 1049-001 Lisboa, Portugal. [4]Department of Organic Chemistry, Faculty of Chemistry, University of Lodz, Tamka 12, 91-403 Lodz, Poland. [5]Department of Cosmetic Raw Materials Chemistry, Faculty of Pharmacy, Medical University of Lodz, Muszyńskiego 1, 90-151 Lodz, Poland. [6]Department of Immunology and Infectious Biology, Institute of Microbiology, Biotechnology and Immunology, Faculty of Biology and Environmental Protection, University of Lodz, Banacha 12/16, 90-237 Lodz, Poland. ✉email: magdalena.wozniczka@umed.lodz.pl; weronika.gonciarz@biol.uni.lodz.pl

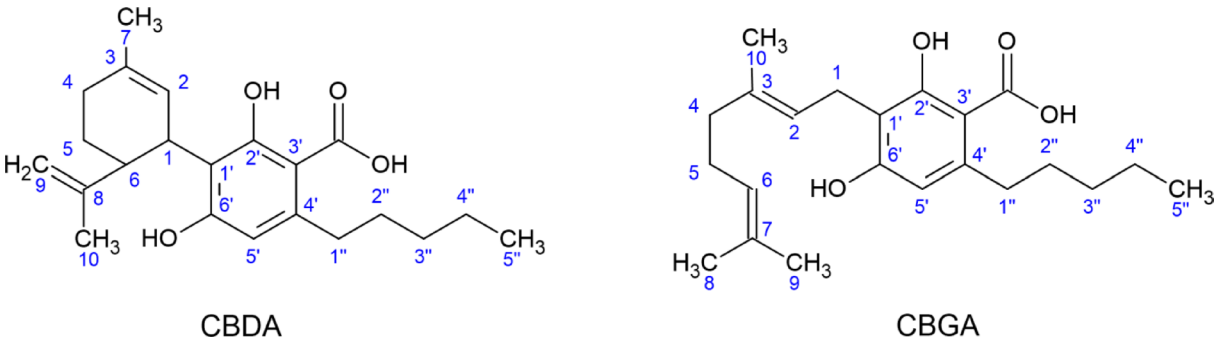

Fig. 1. Structure of the cannabinoid acids.

turn, CBDA is synthesized via cannabidiolic acid synthase (CBDAS), which catalyzes the stereoselective oxidocyclization of cannabigerolic acid (CBGA, Fig. 1) into CBDA[2,4,5]. Literature data suggests that CBDA may be a more bioavailable cannabinoid than CBD, also allowing for better absorption of CBD and its higher serum concentrations at lower doses[6,7].

CBDA is used in creams, foods and beverages, and as a possible treatment for autism. It can induce anti-nausea effects[4,7,8], and the methyl ester of cannabidiolic acid has been shown to be an anti-anxiety agent[9,10]. CBDA induces anti-hyperalgesic responses in the inflammatory pain mode[11] and has been identified as an inhibitor of the migration of highly aggressive breast cancer cells[12]. In addition, it exhibits biological activities, including antioxidant and antimicrobial effects[13].

Antimicrobial activity has also been demonstrated for another non-psychotropic cannabinoid, cannabigerol (CBG) and its precursor (CBGA), suggesting that they have potent antimicrobial properties comparable to CBD and CBDA against various drug-resistant strains of *Staphylococcus aureus*[14]. CBG and CBGA have been shown to have anticholinesterase properties, inducing beneficial effects on cognitive function, including memory and learning. They may also have neuroprotective effects, reducing oxidative stress and inflammation, which are essential factors in the pathogenesis of neurodegenerative diseases[15]. It has even been reported that cannabinoid acids have an antioxidant potential greater than their neutral counterparts[7].

The biological and therapeutic properties of cannabidiol and cannabigerol have been the subject of many publications and are fairly well-identified. In contrast, the pharmacology of CBDA and CBGA is much more limited[4]. The aim of this study was to determine the bacteriostatic and bactericidal effects of cannabinoid acids on multi-resistant *Helicobacter pylori* strains and to investigate the cytotoxic activity of these compounds against gastric cancer. Antimicrobial resistance of *H. pylori* is increasing worldwide and there is concern about the consequences of rising resistance rates, as infection with these bacteria leads to several diseases, including atrophic gastritis, peptic ulcers, mucosa-associated lymphoid tissue lymphoma and gastric cancer[16,17].

The present study attempts to characterize of copper(II) and zinc(II) systems with cannabinoid acids. Transition metal complexes exhibit a variable oxidation state due to uncompleted *d*-subshell and therefore interact with multiple negatively charged ions, which may offer therapeutic possibilities and pharmacological applications[18]. Zn(II) and Cu(II) ions are good candidates for complexation in biological systems due to their superior ability to form stable complexes with biological ligands[19]. Zinc(II) ions are regulatory ions akin to calcium(II) ions and are fundamentally important for cellular control. Zinc is much more widely used than most vitamins as a cofactor in proteins and is involved in the control of cellular metabolism and paracrine and intracrine signaling. It also plays a significant role in biological phosphorylation and redox signalling, affecting cell proliferation, differentiation and death. The roles of zinc(II) ions in cellular regulation, unique among the essential transition metal ions, greatly enhances the importance of zinc for cellular biology tremendously and suggest that the micronutrient zinc has much broader functions than any of the other transition metal ions, including iron[20]. Also copper has received much attention for its enormous biological potential, acting as a cofactor in active sites, participating in a wide range of signalling pathways, such as those associated with pro-proliferative and autophagic kinase pathways involved in oncogenesis[21]. It was found that copper can bind with DNA more frequently than any other divalent cation supporting DNA oxidation. Copper compounds exhibit anticonvulsive, antibacterial, antiinflammatory, antifungal, and antimicrobial activities. In addition, they can be an alternative to platinum-based anticancer drugs due to their lower toxicity and relatively simple mechanism of action[18].

The determination of the chemical properties of both ligands and complexes of biometals in solutions with different pH is a prelude to biological analysis. Chelation clearly alters the biological properties of ligands and metal ions; the newly formed structures can cause many diseases, including cancer, but can also be used to treat them. Processes taking place in solutions provide insight into the different stages of complexation, including their reversibility and competition between reactions. Understanding the structure of complexes is a very important aspect of their biological application[22,23]. Obtaining important information about properties such as solubility or acid–base equilibrium allows the charge state of analytes to be estimated and provides important information on the exact forms that exist under different pH conditions.

Materials and methods

Materials

Cannabidiolic acid (CBDA) and cannabigerolic acid (CBGA) (Fig. 1) were synthesized as described previously[5]. The stock copper(II) nitrate trihydrate and zinc(II) nitrate hexahydrate solutions from Fluka were standardized complexometrically using the disodium salt of ethylenediaminetetraacetic acid in the presence of murexide. The carbonate-free 0.1 M NaOH and ethyl alcohol were purchased from J.T. Baker and POCH, respectively. The HNO_3 solution (Sigma-Aldrich) was standardized alkalimetrically and then determined by the Gran method[24]. The potassium nitrate(V) (J.T.Baker) adjusted the ionic medium. Argon of high purity (Linde) was used.

pH-metric titrations

The potentiometric titrations were performed using a Titrando 905 automatic titrator system (Metrohm) with a combined glass electrode (Metrohm LL Biotrode). The experiments were accomplished in ethyl alcohol-water mixture (50/50, v/v) at a controlled temperature of 25.0 ± 0.1 °C in a thermostatted closed vessel and ionic strength $I = 0.1$ mol/L with KNO_3. Pure argon was passed over the solution surface to ensure the absence of carbon dioxide. The electrode was calibrated with an NaOH titrant on the hydrogen ion concentration using a solution of HNO3 as the substance to be analysed[25]. The protonation constants of the CBDA and CBGA were determined by pH-metric titrations of various concentrations within 2.0–5.0 × 10^{-3} mol L^{-1}, carried out in the pH range of approximately 2.0–12.0. Titrations of the CBDA and CBGA systems in the presence of metal ions, copper(II) or zinc(II), were performed for solutions with metal concentrations of 1.0–2.5 × 10^{-3} mol·L^{-1} and ligand-to-metal molar ratios of 2:1; 3:1. The systems were tested in a pH range of approximately 2.0–12.0. The formation constants of the aqua-hydroxo complexes of copper(II): $[Cu(OH)]^+$, $\log_{10}\beta_{10-1} = -5.94$; $Cu(OH)_2$, $\log_{10}\beta_{10-2} = -12.00$ and zinc(II): $[Zn(OH)]^+$, $\log_{10}\beta_{10-1} = -9.44$; $Zn(OH)_2$, $\log_{10}\beta_{10-2} = -16.42$ were determined under the same conditions and are based on literature data[26,27]. The autoprotolysis constant of the ethanol/water mixture (50/50, v/v) $pK_{ethanol/water} = 13.82$, determined in this work, was also used in the equilibrium model.

Hyperquad 2013 software was used to obtain formation constants from the pH-titration results according to the formula[28,29]: $\beta_{mlh} = [M_mL_lH_h]/[M]^m[L]^l[H]^h$ for $mM + lL + hH \rightleftharpoons M_mL_lH_h$, where L is the CBDA form in the fully deprotonated state. In the case of CBGA, the ligand L takes the form L′ in the above equation. The species distribution curves as a function of pH were calculated using the HySS 2009[30].

Spectrophotometric measurements

Electronic spectra under argon were recorded on a Cary 50 Bio spectrophotometer, slit width 1.5 nm, equipped with a fiber-optic device, dipped directly into the thermostatted titration vessel (temperature kept constant at 25.0 ± 0.1 °C). This allowed the study of equilibrium systems spectrophotometrically, simultaneously with pH measurements controlled by an automatic titrator kit Titrando 905 (Metrohm) with a combined glass electrode (Metrohm LL Biotrode). Before use, the electrode was standardised with pH 4.00 and 7.00 buffers. The pH and ionic strength ($I = 0.1$ M) were adjusted by HNO_3 and KNO_3, respectively. The pH was measured after each addition of carbonate-free NaOH and an appropriate time delay to allow the system to equilibrate. At selected pH values, the spectrum was recorded with a slow scan (300 nm min^{-1}).

The ligands and the Cu(II) complexation equilibria were studied in the wavelength range 200–900 nm, at total ligand concentration 0.9–2.0 × 10^{-3} mol L^{-1}. The Cu(II)–ligand systems were prepared at the ligand-to-metal molar ratio of 2:1. The initial pH was set at around 2.0 in all experiments. The molar absorption coefficients of species have been calculated after deconvolution by HypSpec (part of Hyperquad 2008 suite, Protonic Software)[28].

Electrospray-ionization mass spectrometry (ESI–MS) measurements

Mass spectrometric data were obtained using a Varian 500-MS LC hexapole ion-trap mass spectrometer (Palo Alto, CA, USA) with an accuracy of 0.1 for m/z values. Experiments were performed in positive and negative ion-mode for the copper(II) and zinc(II) systems with CBDA and CBGA in 50/50% (v/v) methanol/water mixture, providing a more stable spray and producing smaller initial droplets than water alone or a high water content solvent[31]. No background electrolyte was added. The concentration of CBDA as well as CBGA was 2.0 × 10^{-3} M in all metal–ligand samples. For the complex systems, the ligand–metal molar ratio was 2:1. Using the species distribution graphs, the samples were provided to different pH values at which the particular complexes and ionic forms of the ligands reached maximum concentrations. The samples were introduced into the ESI–MS source by continuous infusion using an instrument syringe pump at a rate of 10 µL min^{-1}. The ESI-source was operated at 5.00 kV, and the capillary heater was set to 350 °C. The cone voltage was within the range 40,120 V.

Biological assays

Four solutions were used in all bioassays: CBDA, CBGA and their zinc(II) systems with a ligand-to-metal molar ratio of 2:1, all with an initial ethanol/water ratio (50/50, v/v). Tris–HCl/NaCl buffer was used to stabilize the pH at 7.2. The concentrations of complexes in both systems were calculated using HySS simulation.

Cytotoxicity assay

In vitro cell culture studies were performed with Hs68 skin fibroblasts (CRL-1635™, American Type Cell Cultures (ATCC), Rockville, MD, USA) and human AGS (CRL-1739) gastric adenocarcinoma epithelial cell line obtained from the ATCC (Rockville, Md.) to investigate their viability upon exposure to CBDA, CBGA, Zn-CBDA and Zn-CBGA. The cells were cultured at 37 °C in a 5% CO_2 in Roswell Park Memorial Institute (RPMI)-1640 medium (AGS cell lien) or high glucose RPMI-1640 medium (Hs68 fibroblasts) supplemented with 10% heat-inactivated fetal bovine serum (FBS), and standard antibiotics: penicillin (100 U/mL) and streptomycin (100 µg/mL) (all cell culture components were from Biowest, Nuaillé, France). The cell line (density of 2 × 10^5 cells/

mL) according to the ISO norm 10993-5 (International Organization for Standardization, 2009; Biological evaluation of medical devices—Part 5: Tests for in vitro cytotoxicity), based on the 3-(4,5-dimethylthiazol-2-yl)-2,5-diphenyltetrazolium bromide (MTT) reduction test, as previously described[32]. Test samples were diluted in a complete culture medium and were used in the following concentrations: 2.0×10^{-3} M, 1.0×10^{-3} M, 0.5×10^{-3} M, 0.25×10^{-3} M, 0.1×10^{-3} M, 0.05×10^{-3} M, 0.025×10^{-3} M, and 0.01×10^{-3} M. Cell cultures in the medium alone, without the tested materials, were used as a positive control (PC) for cell viability. In contrast, cells treated with 0.03% H_2O_2 were used as a negative control (NC), i.e., 100% dead cells due to cell lysis. The absorbance was measured spectrophotometrically using a Multiskan EX plate reader (Thermo Scientific, Waltham, MA, USA) at 570 nm. MTT reduction relative to untreated cells (%) = (absorbance of treated cells/absorbance of untreated cells × 100%) − 100%. The MTT reduction test mentioned above was performed in three independent experiments.

Assessment of apoptosis, DNA damage, and AGS cell proliferation

AGS cells were cultured as described above. Cells were not stimulated (culture only in culture medium) or stimulated as follows: for 24 h with CBDA, CBGA, Zn-CBDA, and Zn-CBGA were used in the following concentration 0.05×10^{-3} M; doxorubicin (Dox) at the concentration 2 µg/mL was used as a positive control. According to the manufacturer's procedure, apoptosis was also determined by terminal deoxynucleotidyl transferase dUTP nick end labeling (TUNEL) assay (Thermo Fisher Scientific, Waltham, MA, USA). DNA damage was determined using primary antibody against phosphorylated H2AX (Ser139) (Thermo Fisher Scientific, Waltham, MA, USA), which is induced in response to double-strand breaks (DSB), as previously described[33,34]. TUNEL and DNA damage results were shown in relative fluorescence units (RFU). The fluorescence intensity was measured using a multifunctional spectrophotometer SpectraMax i3 (Molecular Devices, San Jose, CA, USA). Three independent experiments were performed in triplicate.

Cell proliferation of human AGS cells after stimulation with tested components, as described above, was evaluated using a commercial CyQUANT™ Cell Proliferation Assay (Invitrogen™, Thermo Fisher Scientific, Waltham, MA, USA). Cells were washed with phosphate-buffered saline (PBS) and frozen at − 80 °C. Samples were thawed at room temperature, and cells were lysed in a buffer containing CyQUANT prepared according to the manufacturer's instructions. Fluorescence was measured at an emission wavelength of 550 nm and excitation wavelength of 590 nm using a SpectraMax i3x Multi-Mode Microplate Reader (Molecular Devices, San Jose, CA, USA). Results were shown in relative fluorescence units (RFU). The fluorescence intensity was measured using a multifunctional spectrophotometer SpectraMax i3 (Molecular Devices, San Jose, CA, USA). Three independent experiments were performed in triplicate.

Assessment of antimicrobial activity

The antimicrobial efficiency of CBDA, CBGA, Zn-CBDA, and Zn-CBGA, applied at the following concentrations: 0.1×10^{-3} M, 0.05×10^{-3} M, 0.025×10^{-3} M and 0.01×10^{-3} M, was carried out against three reference *H. pylori* strains: ATTC 700,392, CCUG (Culture Collection University of Gothenburg, Sweden) 17,874 and 700,392, and five clinical *H. pylori* strains: 1—(no resistant), 2—(resistant to metronidazole), 3—(resistant to metronidazole and levofloxacin), 4—(resistant to clarithromycin and metronidazole), 5—(resistant to clarithromycin) and 6—(resistant to clarithromycin) from the collection of clinical strains, Medical University of Wrocław, Poland. According to previously described methods, the broth microdilution assay determined the antibacterial activity of tested formulations according to The European Committee on Antimicrobial Susceptibility (EUCAST) recommendations[35]. The antimicrobial activity of these formulations was evaluated based on their minimal inhibitory concentration (MIC) or minimal bactericidal concentration (MBC). The tests mentioned above were performed in three independent experiments.

Statistical analyses

Graphs were prepared using GraphPad Prism 10.0 software (https://www.graphpad.com/, GraphPad Software Inc., San Diego, CA, USA). Data were expressed as median values ± range. The differences between groups were tested using the non-parametric U Mann–Whitney test. The Statistica 13 PL software (https://statistica.software.informer.c.m/13.3software, Kraków, Poland) was used for statistical analysis. Results were considered statistically significant when $p < 0.05$). We used the Shapiro–Wilk test (S–W) to assess normality distribution.

Results and discussion

Protonation equilibria of the studied ligands

The wide pH range of CBDA potentiometric titration allows the determination of three protonation constants (Table 1). The individual ionic forms of the ligand are presented in the pH-dependent species distribution diagram (Supplementary Fig. S1). Despite the ethanol–water environment, the acidity of -COOH is of the same order as that of other compounds containing this group[36,37]. UV–Vis absorption spectra in the pH range 2.63 to 4.35, i.e. after deprotonation of the carboxyl group, displayed shoulder formation at around 420 nm (Supplementary Fig. S2a). The appearance of an isosbestic point (470 nm) at pH 4.50 indicates an equilibrium change from the $[LH_2]^-$ form to the $[LH]^{2-}$, confirming the deprotonation of the first hydroxyl group ($pK_{a2CBDA} = 4.95$). The hydroxyl oxygen deprotonation is also accompanied by a colour change from yellow to pink. It is confirmed by the calculation result in the HypSpec program, in which the forms of the ligand were determined together with their molar absorption coefficients (Table 1, Supplementary Fig. S2c). It can be assumed that pK_{a2CBDA} refers to the OH^- in the 6′-position, as its acidity is most likely higher than that of the OH^- group in the 2′-position. This is influenced by the formation of a stable intramolecular hydrogen bond between the carbonyl of the carboxyl group and the vicinal hydroxyl group[5,7,38].

Species	$log_{10}\beta$	Stepwise dissociation constants	λ_{max} (ε_{max})
$[L]^{3-}$			~540[sh] (63)
$[LH]^{2-}$	11.68(7) (2′-OH)	pK_{a3CBDA} 11.68	~570[sh] (12)
$[LH_2]^{-}$	16.63(16) (6′-OH)	pK_{a2CBDA} 4.95[b]	~420[sh] (23)
$[LH_3]$	18.66(28) (COOH)	pK_{a1CBDA} 2.02[c]	
σ; n[a]	49.23; 781		
$[L'H]^{2-}$	11.88(8) (2′-OH)	pK_{a2CBGA} 11.88	
$[L'H_2]^{-}$	16.89(24) (6′-OH)	pK_{a1CBGA} 5.01[d]	~425[sh] (52)
σ; n[a]	43.96; 219		
$[CuLH_{-1}]^{2-}$	2.74(26)		~525[sh] (220)
σ; n[a]	8.99; 781		
$[ZnLH_{-1}]^{2-}$	0.82(4)		
σ; n[a]	6.57; 260		
$[CuL'H_{-1}]^{2-}$	2.48(16)		
σ; n[a]	4.65; 103		
$[ZnL'H_{-1}]^{2-}$	1.30(6)		
σ; n[a]	12.25; 190		

Table 1. Decimal logarithms of overall protonation and formation constants for CBDA, CBGA and their Cu(II) and Zn(II) systems, $\beta_{mlh} = [M_mL_lH_h]/[M]^m[L]^l[H]^h$ and $\beta_{ml'h} = [M_mL'_lH_h]/[M]^m[L']^{l'}[H]^h$ at 25.0 ± 0.1 °C, $I = 0.1$ (KNO_3) and UV–Vis spectral data. Standard deviations in parentheses after overall protonation and stability constants refer to random errors only. [a]σ—the value of the normalized sum of squared residuals; n—number of titration points. [b]$pK_{a2CBDA} = \log_{10} K^{LH}_{LH_2} = \log \beta_{LH_2} - \log \beta_{LH}$ [c]$pK_{a1CBDA} = \log_{10} K^{LH_2}_{LH_3} = \log \beta_{LH_3} - \log \beta_{LH_2}$ [d]$pK_{a2CBGA} = \log_{10} K^{L'H}_{L'H_2} = \log \beta_{L'H_2} - \log \beta_{L'H}$

Further alkalization of the solution led to a shift of the spectral curves towards higher wavelengths, accompanied by a deepening of the pink colour of the titrated solution (Supplementary Fig. S2b). HypSpec deconvolution allowed calculating the molar absorption coefficient with shoulder peak at about 540 nm for the completely deprotonated ligand $[L]^{3-}$ (Table 1, Supplementary Fig. S2c). This form is the result of the dissociation of the hydroxyl group at the 2′-position ($pK_{a3CBDA} = 11.68$). Since, to our knowledge, the values of three dissociation constants for the cannabidiolic acid have not been previously determined, it is not possible to compare the obtained constants. However, these constants are found similar to those assigned to the hydroxyl groups present in other compounds in alcohol-water medium[39,40].

For the second ligand, CBGA, calculations confirmed two dissociation constants related to the hydroxyl groups, equal to $pK_{a1CBGA} = 5.01$ and $pK_{a2CBGA} = 11.88$ (Table 1). In acidic media up to pH 4.5, a white–yellow precipitation was observed, probably due to the insoluble form of the ligand. This meant that the pH conditions required to dissociate the proton from the carboxyl group could not be determined. In slightly-acidic environment, the precipitation changed to a pale yellow solution and then to a pink colour. As shown in Table 1, the basicity of the hydroxyl groups of CBGA is higher than that of the CBDA ligand. The slight pK_a differences are consistent with the electronic effects of the substituents attached to the benzene ring. The electron donating potential of the aliphatic chain in the CBGA increases the electron density on the oxygen atoms, resulting in more basic pK_a values for the CBGA donor groups than CBDA[29,41]. Dissolution of precipitation above pH 4.57 allowed electron absorption spectra to be recorded for CBGA (Supplementary Fig. S3a). Above pH 11.14, the absorbance feature at ca 410 nm was revealed. Based on the potentiometric results (Supplementary Fig. S1b), this most likely corresponds to deprotonation of the second OH group and formation of the $[L']^{3-}$. However, for only one ligand form with a dissociated carboxyl group, $[L'H_2]^{-}$, HypSpec deconvolution enabled the calculation of the molar absorption coefficients (Table 1, Supplementary Fig. S3b).

Complex formation equilibria

Cu(II) complexes

Potentiometric titrations in the presence of the metal ion confirmed the formation of one complex for each copper(II) system with both CBDA (Fig. 2a) and CBGA (Fig. 2b). The stability constants of the designated complexes are given in Table 1. Initially, in the Cu(II)-CBDA system, the solution was pale yellow, then above pH 2.9, precipitation was observed, which changed colour from white to green. As the ligand alone is soluble in this pH range, the precipitation can be attributed to forming insoluble copper(II) complexes with CBDA. Above pH 10, the precipitation dissolved and, during titration, the solution turned pink, indicating the presence of uncoordinated forms of the ligand with deprotonated hydroxyl groups. Also, in the spectrophotometric measurements, the pink colouration of the solution at pH about 12 was accompanied by the appearance of an isosbestic point (at 600 nm) and a shoulder peak formation at around 530 nm (Supplementary Fig. S4). A similar spectrum has previously been recorded for CBDA alone for its $[L]^{3-}$ form (Supplementary Fig. S2b).

The conditions for the formation of the $[CuLH_{-1}]^{2-}$ complex, i.e. pH above 10, favour the deprotonation of all the donor groups in cannabidiolic acid, as well as the deprotonation of the coordinated water molecule. Therefore, the most likely ligand binds with the central ion in the equatorial sites via 2′-hydroxyl and carboxyl

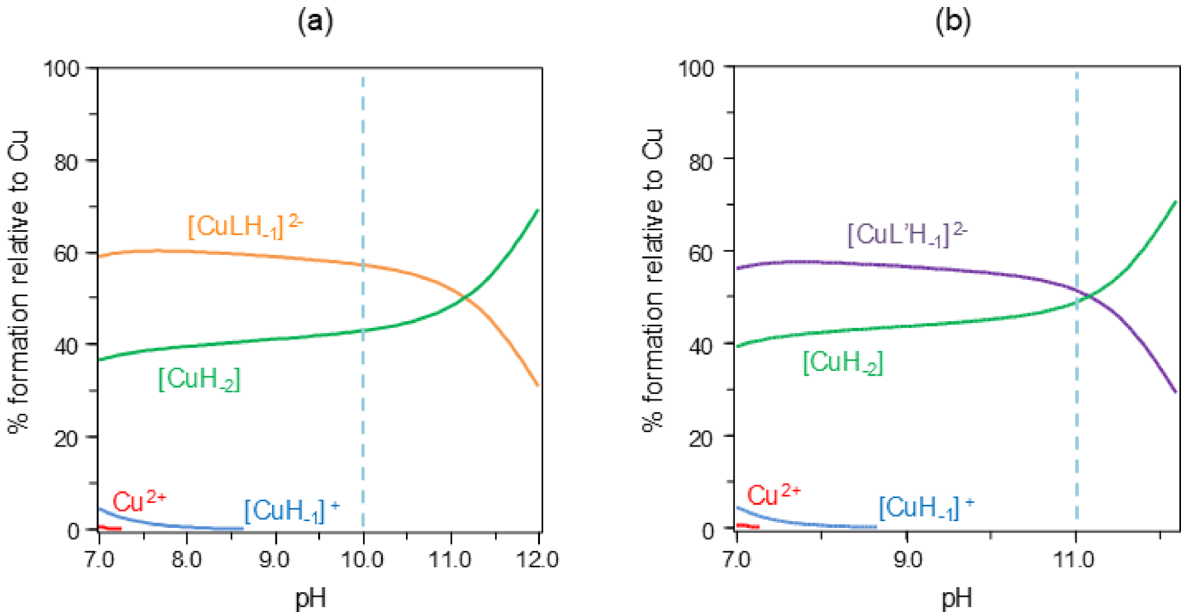

Fig. 2. Species distribution curves for the complexes formed in the (**a**) Cu(II)-CBDA and (**b**) Cu(II)-CBGA systems at ligand-to-metal molar ratio 2:1 as a function of pH relative to Cu(II); $C_{CBDA/CBGA} = 2.0 \times 10^{-3}$ M. The dashed line indicates the pH below which precipitation was observed.

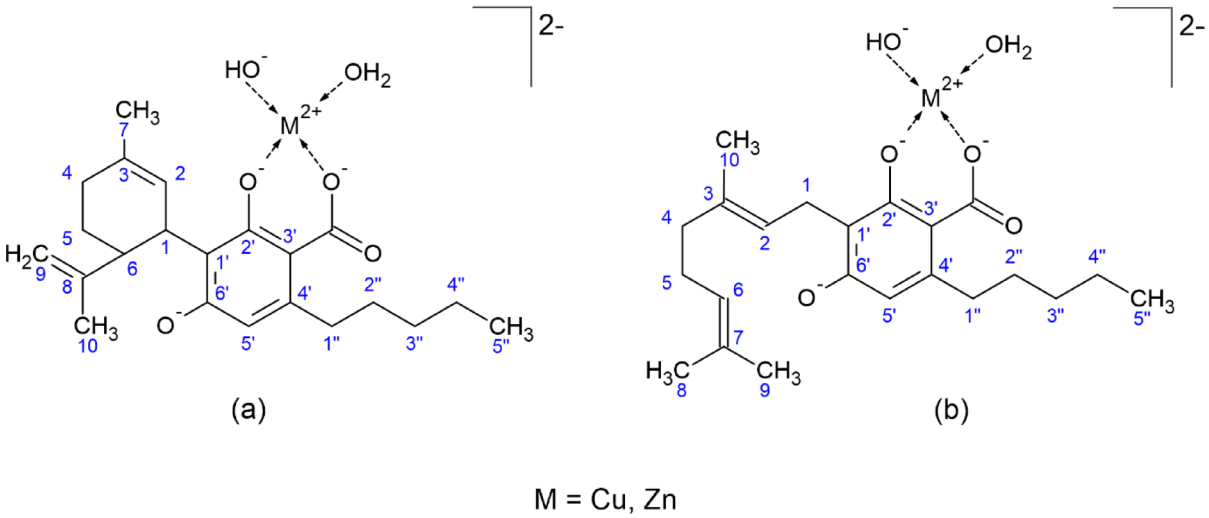

Fig. 3. Proposed coordination modes of complexes in systems with (**a**) CBDA and (**b**) CBGA.

groups forming a six-membered chelate ring (Fig. 3a). Moreover, one position is occupied by deprotonated water, creating a hydroxide complex. After introducing additional complexes with more deprotonated water molecules into the computational model, the experimental potentiometric curve did not coincide with the theoretical curve, thus not confirming the formation of such forms.

The electronic absorption spectra also indicate the formation of the $[CuLH_{-1}]^{2-}$ complex, confirmed by HypSpec deconvolution (Supplementary Fig. S4b). The maximum molar absorption coefficient is given in Table 1. A weak shoulder peak is visible at around 380 nm in a strongly alkaline environment, suggesting deprotonation of the hydroxyl group[36,42].

In the case of the Cu(II)-CBGA system, the precipitation also started to form in an acidic medium (above pH 2.6) and dissolved at a pH of around 11. The colour changes were analogous to the system with CBDA. The narrow measuring range allowed the $[CuL'H_{-1}]^{2-}$ complex to be determined exclusively by potentiometric method (Table 1, Fig. 2b). As the molar absorption coefficients were only determined for one form of the CBGA ligand (Table 1), this probably precluded the calculation of coefficients for the complex alone. Nevertheless, the similarity of the UV–Vis spectra and stability constants of the complexes of both ligands suggests that the coordination of Cu(II) ions and tridentate cannabigerolic acid resulted in a structure analogous to the

$[CuLH_{-1}]^{2-}$ complex (Fig. 3b). Electron absorption spectra for the Cu(II)-CBGA system above pH 12.5 showed the maximum absorbance at about 490 nm (Supplementary Fig. S5), which most likely corresponds to the form of the fully deprotonated ligand (Supplementary Fig. S3a), as in the Cu(II)-CBDA system.

The ESI–MS spectra for the Cu(II)–CBDA system were taken at three pH values (2.1, 10.0, 11.7) (Supplementary Fig. S6). At pH 10.0, the presence of the copper(II) complex ($m/z = 351.4$ and $m/z = 353.4$ for isotopes Cu^{63} and Cu^{65}, respectively) with a fragment ion was detected in the positive-ion ligand spectra. Fragmentation of the ligand occurred due to the loss of two methyl groups and chain at the 6-position.

The ESI–MS spectra of the Cu(II)–CBGA system also showed the formation of different species containing copper(II) ions depending on the pH (Supplementary Fig. S7). In acidic medium, the trace signals of $[CuL'H_2]^+$ complex ($m/z = 422.4$; 424.4) and its positive adducts ($m/z = 407.4$; 409.4) appeared with fragment ion due to loss of methyl group. The complex with the protonated ligand molecule was not confirmed by potentiometric and spectrophotometric studies, probably due to its low content in solution in a very acidic medium and subsequent precipitation over a wide pH range. At pH 11.01, the further bi-H^+ adduct of Cu(II) complex corresponding to $m/z = 353.4$; 355.4 was detected. The species contains a fragment ion obtained from $[L']^{3-}$ by detaching two methyl groups and an aliphatic chain at the 6-position.

Zn(II) complexes

As shown in the speciation diagrams for zinc(II) systems with cannabinoid acids (Fig. 4), the environmental conditions of complex formation, as well as the metal-promoted deprotonation, favour the dissociation of both ligands and water molecule. Thus, by analogy with the copper(II) system, it can be assumed that the ligands coordinate in the same way with zinc(II) ions to form hydroxide complexes (Fig. 3). However, according to the Irving-Williams series, stability constants of Zn(II) complexes, shown in Table 1, reach lower values. In the case of the Zn(II)–CBDA system, the light yellow solution was observed up to a pH of about 2.5, which changed to white and pink precipitation. Above pH 7, the precipitation dissolved, and the solution became transparent and then pale pink, indicating complete deprotonation of the ligand. In the presence of CBGA, the system behaved similarly to Zn(II)-CBDA, except that a precipitate formed from the beginning of the titration (pH around 2.2). In Zn(II) solutions, the predominant forms are $[ZnLH_{-1}]^{2-}$ and $[ZnL'H_{-1}]^{2-}$, and, in contrast to Cu(II) systems with cannabinoid acids, only trace amounts of zinc(II) aqua-hydroxo complexes are observed (cf. Figures 2a,b, 4a,b).

In the ESI–MS spectra of the Zn(II)-CBDA system (Supplementary Figs S8, S9), the zinc(II) complex with one fully deprotonated CBDA molecule, $[Zn + L + 2H]^+$ with $m/z = 422.4$, was observed at pH 7.5, confirming the potentiometric data. Interestingly, the ESI–MS studies revealed complexes with two and three ligand molecules: $[Zn + 2L + H + 4Na]^+$, $m/z = 868.8$, $[Zn + 2L + H + 2Na]^-$, $m/z = 822.8$ and $[Zn + 3L + 6H]^-$, $m/z = 1137.2$. The presence of these complexes in the model did not allow potentiometric data fitting, but the ESI–MS spectra indicated their stability under ionization conditions.

In an attempt to confirm the presence of the complexes in the Zn(II)-CBGA system, ESI–MS spectra at pH 7.7 and 11.4 were collected in positive- and negative-ion mode (Supplementary Figs S10, S11). The mononuclear complex with one ligand molecule were observed in a strongly alkaline medium: $[Zn + L' + H + Na]^+$, $m/z = 446.4$. The bi-ligand complexes: $[Zn + 2L' + H + 4Na]^+$, $m/z = 872.8$ and $[Zn + 2L' + H + 2Na]^-$, $m/z = 826.8$, mainly showed lower relative intensity over the pH range tested.

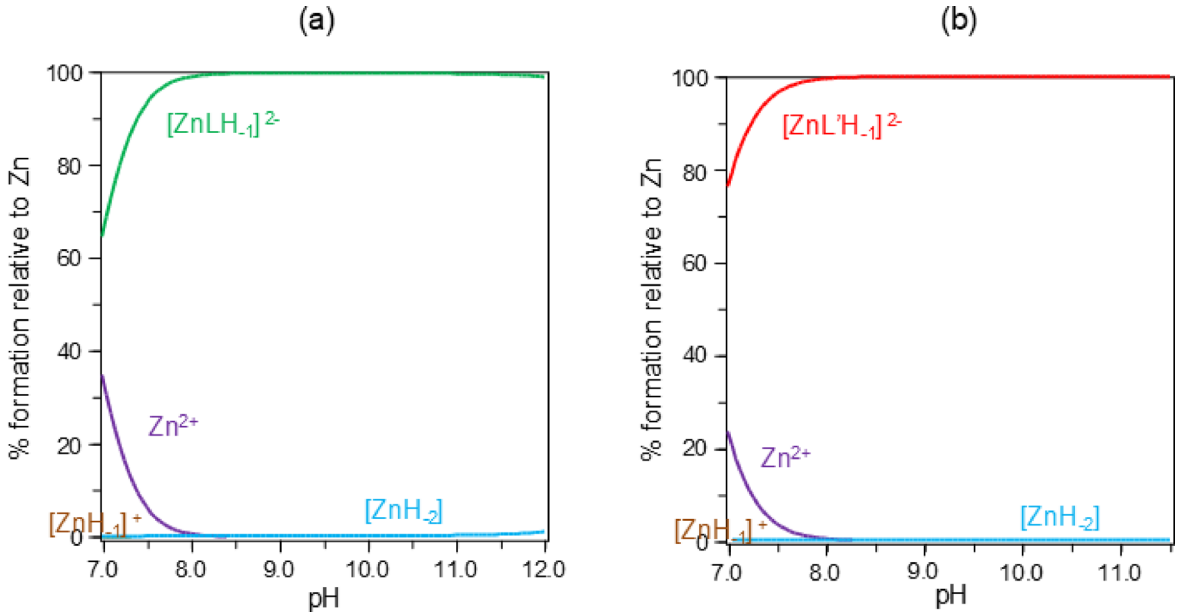

Fig. 4. Species distribution curves for the complexes formed in the (**a**) Zn(II)-CBDA and (**b**) Zn(II)-CBGA systems at ligand-to-metal molar ratio 2:1 as a function of pH; $C_{CBDA/CBGA} = 2.0 \times 10^{-3}$ M.

Biological activity

In this study, human Hs68 fibroblasts were examined for cytotoxicity assessment of tested CBDA, CBGA, Zn-CBDA and Zn-CBGA solutions. Due to the documented anti-cancer effects of CBD and CBG[43,44], we also tested the cytotoxicity properties of CBDA, CBGA, Zn-CBDA and Zn-CBGA solutions against human gastric cancer cell line AGS. Based on potentiometric studies of zinc(II) systems (Supplementary Fig. S12), both $[ZnLH_{-1}]^{2-}$ and $[ZnL'H_{-1}]^{2-}$ complexes and zinc(II) ions themselves were observed at physiological pH.

The influence of all tested materials on the viability of the Hs68 fibroblasts and gastric cancer cells AGS was assessed by MTT reduction assay, based on the measurement of mitochondrial dehydrogenase activity in the presence or absence of the tested substances. The colour intensity of dissolved formazan crystals corresponds to the metabolic activity of tested cells. The viability of Hs68 cells incubated in the presence of CBDA, CBGA, Zn-CBDA and Zn-CBGA was higher than 70%, meeting the biological safety standard (for concentrations equal to and below 0.05×10^{-3} M) (Fig. 5). For comparison CBDA, CBGA at the concentration equal to 0.05×10^{-3} M towards AGS has cytotoxic properties, whereas Zn-CBDA and Zn-CBGA at the same concentration meet biological safety standards (Fig. 5). Our results indicated a better cytotoxic effect of phytocannabinoids against gastric cancer cells that is the case for colon cancer cells, for which the IC50 value was 13.13 IC50 µM/mL for CBD, 24.14 µM/mL for CBG and 22.86 µM/mL for CBGA[44].

Considering that CBDA and CBGA at a concentration of 0.05×10^{-3} M are safe for healthy cells but remain cytotoxic to cancer cells and are resistant to an acidic environment (potentiometric and spectroscopic measurements), we decided to check the effect of CBDA, CBGA, Zn-CBDA and Zn-CBGA solution on apoptosis, DNA damage and proliferation of AGS cancer cells (Fig. 6).

Cannabinoids exhibit anticancer potential through several strategies, such as enhancing apoptosis-mediated cell death, inhibiting cell proliferation, impairing angiogenesis in tumour cells, and blocking invasion and metastasis[45]. We show that Zn-CBDA and Zn-CBGA at a concentration of 0.05×10^{-3} M statistically significantly induce apoptosis and DNA damage and inhibit AGS cell proliferation (Fig. 6).

CBD has been tested in several cancer studies. It was the first non-toxic exogenous cannabinoid to reduce the tumour aggression in metastatic breast cancer cells[46]. Cannabinoid-induced apoptosis in C6 glioma cells is the cancer cell line type used in most cannabinoid antitumor activity research. Cannabinoids also exhibit antiproliferative effects in breast and skin cancer cells by activating CDK (cyclin-dependent kinase) inhibitors,

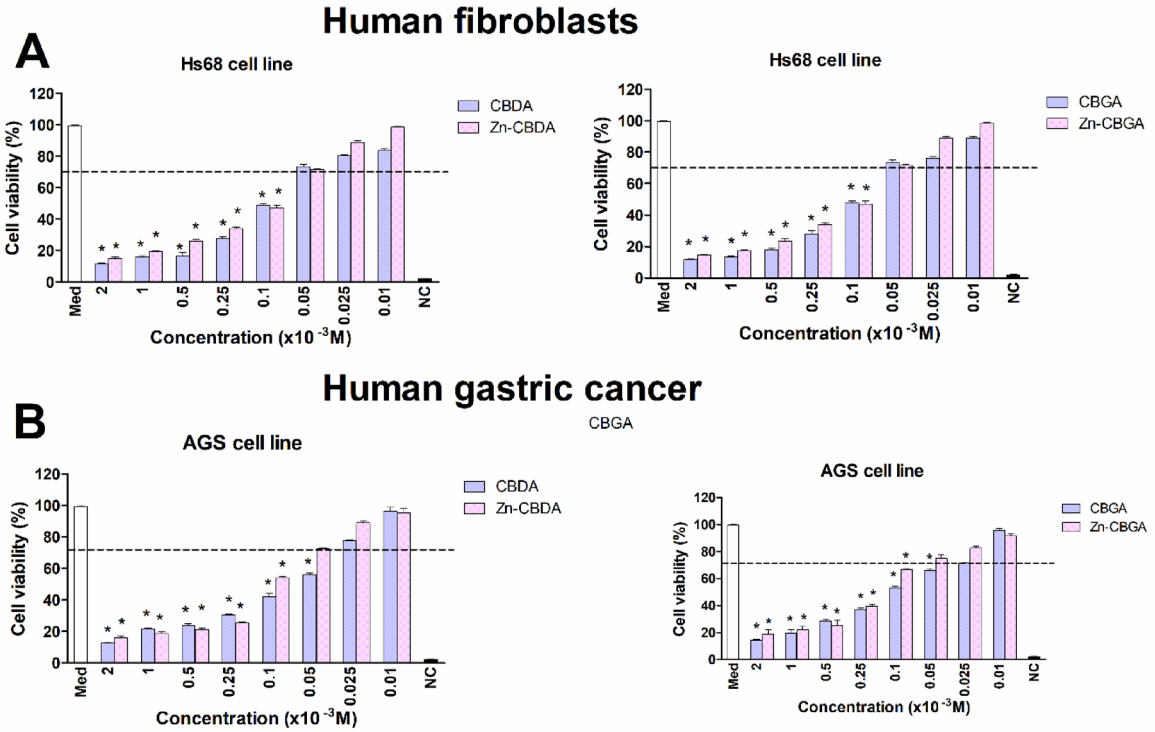

Fig. 5. The influence of CBDA, CBGA, Zn-CBDA and Zn-CBGA on cell viability in MTT reduction assay. Cell viability of human fibroblasts (**A**) and human gastric cancer AGS (**B**) was estimated as the percent of cells that were able to reduce tetrazolium salt (3-(4,5-dimethylthiazol-2-yl)-2,5-diphenyltetrazolium bromide) (MTT). NC—negative control (cells treated with 0.03% H_2O_2), PC-positive control (cells in medium alone). Results are shown as mean ± standard deviation (SD), N = 3. The black line indicates the minimal percentage of viable cells (70%) required to confirm the biomaterial as non-cytotoxic in vitro. Statistical analysis was performed using the nonparametric U Mann–Whitney test with significance, $p < 0.05$ (*unstimulated cells vs. stimulated cells).

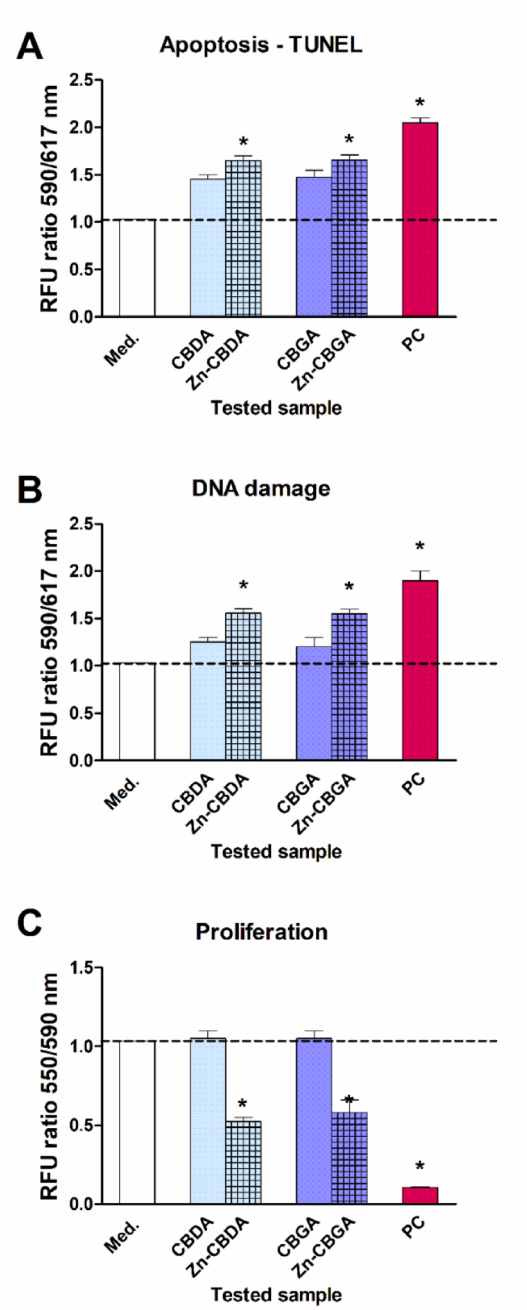

Fig. 6. The influence of CBDA, CBGA, Zn-CBDA and Zn-CBGA solutions at the concentration 0.05×10^{-3} M on cell apoptosis (**A**), DNA damage (**B**) and proliferation (**C**) in cell cultures of human gastric cancer cells AGS. The positive control (PC) consisted of cells treated with doxorubicin at a 2 µg/mL concentration. The results of three independent experiments performed in triplicates for each experimental variant are presented. Statistical analysis was performed using the nonparametric U Mann–Whitney tests with significance for * unstimulated (only medium) versus stimulated.

p21 and p27, and phosphorylating retinoblastoma protein. This, in turn, inhibits the cell cycle and triggers programmed cell death[47].

One of the factors promoting the development of stomach cancer is infection with the *H. pylori* bacteria, which also causes gastric and duodenal ulcers[48]. They are on the WHO list of carcinogens and may be involved in developing systemic diseases[49]. Induction of oxidative stress and apoptosis in gastric tissue and diminishing activity of immune cells by these bacteria may result in the maintenance of infection[34,50]. The resistance of *H. pylori* to antibiotics (clarithromycin, levofloxacin, metronidazole) has become a problem[51]. In 2017, the WHO recommended searching for new bactericidal substances towards *H. pylori* or substances with

Helicobacter pylori strains	MIC/MBC ($\times 10^{-3}$ M)								Tested drug
	CBDA		CBGA		Zn-CBDA		Zn-CBGA		
	MIC	MBC	MIC	MBC	MIC	MBC	MIC	MBC	
Reference strains									
H. pylori ATCC 700,392	0.01	0.25	0.01	0.25	0.05	0.01	0.05	0.01	Sensitive to amoxixillin, metronidazole, levofloxacin, metronidazole
H. pylori CCUC 17,874	0.01	0.25	0.01	0.25	0.05	0.01	0.05	0.01	Sensitive to amoxixillin, metronidazole, levofloxacin, metronidazole
Clinical strains									
H. pylori 1	0.01	0.25	0.01	0.25	0.025	0.025	0.025	0.025	Sensitive to amoxixillin, metronidazole, levofloxacin, metronidazole
H. pylori 2	0.01	0.25	0.01	0.25	0.025	0.025	0.025	0.025	Resistant to metronidazole
H. pylori 3	0.01	0.25	0.01	0.25	0.025	0.025	0.025	0.025	Resistant to metronidazole and levofloxacin
H. pylori 4	0.01	0.25	0.01	0.25	0.025	0.025	0.025	0.025	Resistant to clarithromycin and metronidazole
H. pylori 5	0.01	0.25	0.01	0.25	0.025	0.025	0.025	0.025	Resistant to clarithromycin
H. pylori 6	0.01	0.25	0.01	0.25	0.025	0.025	0.025	0.025	Resistant to clarithromycin

Table 2. Antimicrobial activity of CBDA, CBGA, Zn-CBDA and Zn-CBGA is shown as minimal inhibitory concentration (MIC) and minimal bactericidal concentration (MBC).

immunomodulatory activity to enhance the immune mechanism of the host. Due to the above, we checked the minimum inhibitory concentration (MIC) and minimum bactericidal concentration (MBC) of CBDA, CBGA, Zn-CBDA and Zn-CBGA against two *H. pylori* reference strains and clinical strains with resistance to standard antibacterial drugs.

As indicated in Table 2, for the CBDA and CBGA ligands, the MIC values against *H. pylori* reference and clinical strains are equal to 0.01×10^{-3} M (non-toxic concentration), while the MBC values are equal to 0.25×10^{-3} M. As presented in the Martinenghi et al. study, CBDA showed no bacterial inhibitory activity against other Gram-negative strains, even at concentrations 20 times higher[52]. Natural anti-*H. pylori* compounds–anthraquinones and anthraquinone glucosides – isolated from the *Rumex acetosa* showed MIC values ranging from about 0.003 to 0.025×10^{-3} M. For comparing, metronidazole, used as an antibiotic in clinical field for a gastric ulcer, had lower MIC value (0.003×10^{-3} M), but some strains are resistance to it. Quercetin, a natural urease inhibitor, has potential as a valuable agent against H. pylori and is used as a positive control with a MIC of 0.05×10^{-3} M[53,54].

The Zn-CBDA and Zn-CBGA have stronger antibacterial properties. The MIC values against reference and clinical strains of *H. pylori* are equal to 0.05×10^{-3} M and 0.025×10^{-3} M, respectively, while the MBC values are equal to 0.01×10^{-3} M and 0.025×10^{-3} M (Table 2); both concentrations are safe for both healthy human fibroblasts and AGS gastric cancer cells (Fig. 5). Bismuth-based drugs have been used as the first-line treatment against *H. pylori*. For comparison with Zn(II) species, the antimicrobial activity of Bi(III) complexes supported by pyridine-2,6-dicarboxylate, oxalate and thiourea showed MIC values in the range of 0.006×10^{-3}–0.03×10^{-3} M[55]. The excellent MIC and MBC values of Zn-CBDA and Zn-CBDG may cause a "Trojan horse" effect using the siderophore produced by bacterial transporters[56]. In addition, a hydroxyl group in the ligands can influence their antimicrobial activity, which is related to the interaction with the cell membrane of microorganisms[57]. Thus, antibiotic effectivity of the CBDA and CBGA suggests that the antibacterial pharmacophore falls on the resorcinol moiety of this cannabinoid and not the terpenoid and n-pentyl groups functioning as modulators for lipophilicity. Interestingly, in the Appendino et al. study, olivetol showed moderate activity against the tested bacterial strains, while resorcinol alone exhibited no activity. This suggests the presence of the pentyl chain and the monoterpene molecular group significantly increases the activity of resorcinol[14,52].

Conclusion

The protonation properties of cannabinoid acids (cannabidiolic and cannabigerolic acids) in ethanol–water mixture (50/50, v/v) were confirmed using potentiometric and spectroscopic methods. Two protonation constants associated with the hydroxyl groups were determined for both ligands, with the electronic effects of the substituents attached to the benzene ring influencing the higher basicity of the CBGA hydroxyl groups compared to CBDA. Due to the precipitation in an acidic environment in the CBGA solution, only the deprotonation constant of the carboxyl group of the CBDA ligand could be examined.

The formation of the complex with one ligand molecule was confirmed for each metal system by potentiometric and ESI–MS measurements and supported by UV–Vis studies in the case of copper(II) species. The stability constants were calculated for all structures, with the constants showing lower values for the zinc(II) system, in accordance with the Irving-Williams series. The occurrence of precipitation over a wide pH range in all ethanol–water solutions limited the determination of other soluble complexes. Only ESI–MS studies revealed that zinc(II) complexes with two and three ligand molecules are stable under ionisation conditions, but most of these species showed low relative intensity. The formation of the species in an alkaline medium involved deprotonation of all donor groups and allowed the coordination of cannabinoid acids most likely by equatorial sites through 2′-hydroxyl and carboxyl groups in the form of a six-membered chelate ring. In addition, deprotonation of the bound water molecule led to the formation of hydroxide complexes.

Based on bioassays, the ligands demonstrated cytotoxic properties against the human gastric cancer cell line AGS at concentrations that are safe for healthy cells. In contrast, zinc(II) systems with these ligands complied

with biosafety standards. At concentrations that demonstrated biological safety, the ratio of the ethyl alcohol-water mixture obtained by dilution was approximately 1/99, v/v, which caused these solutions to be non-toxic in vitro. The development of gastric disease has been associated with *Helicobacter pylori* infection, with chronic inflammation predisposing individuals to the onset of gastric cancer. Therefore, searching for new compounds exhibiting bactericidal activity against these strains is crucial. Analyses against *H. pylori* revealed that the CBDA and CBGA ligands displayed inhibitory activity against reference and clinical strains of this bacterium. Zinc(II) complexes possess more pronounced antimicrobial properties, illustrating a significant bactericidal capacity in addition to their inhibitory effects. The action of these complexes may be predicated on a "Trojan horse" effect utilising the siderophore produced by bacterial transporters.

CBDA, CBGA and their complexes with zinc(II), thanks to their inhibitory and bactericidal properties against *H. pylori* with simultaneous targeting against the development of the human gastric cancer cell line AGS, could be used as a basis for the development of new formulations to combat gastric diseases. Importantly, these compounds are safe for healthy cells under the conditions in which they exert their antimicrobial and cytotoxic effects.

Data availability

Data will be made available on request. Data are available from the corresponding authors.

Received: 12 March 2025; Accepted: 20 May 2025
Published online: 28 May 2025

References

1. Merrick, J. et al. Identification of psychoactive degradants of cannabidiol in simulated gastric and physiological fluid. *Cannabis Cannabinoid Res.* **1**(1), 102–112 (2016).
2. Simei, J. L. Q. et al. Research and clinical practice involving the use of cannabis products, with emphasis on cannabidiol: A narrative review. *Pharmaceuticals* **17**, 1644 (2024).
3. De Vita, S. et al. Phytochemical analysis of the methanolic extract and essential oil from leaves of industrial hemp *Futura 75* cultivar: isolation of a new cannabinoid derivative and biological profile using computational approaches. *Plants* **11**, 1671 (2022).
4. Pertwee, R. G. et al. Cannabidiolic acid methyl ester, a stable synthetic analogue of cannabidiolic acid, can produce 5-HT_{1A} receptor-mediated suppression of nausea and anxiety in rats. *Br. J. Pharmacol.* **175**, 100–112 (2018).
5. Formato, M. et al. (-)-Cannabidiolic acid, a still overlooked bioactive compound: An introductory review and preliminary research. *Molecules* **25**, 2638 (2020).
6. Wakshlag, J. J. et al. Pharmacokinetics of cannabidiol, cannabidiolic acid, Δ9-tetrahydrocannabinol, tetrahydrocannabinolic acid and related metabolites in canine serum after dosing with three oral forms of hemp extract. *Front. Vet. Sci.* **7**, 595 (2020).
7. Boulebd, H. Is cannabidiolic acid an overlooked natural antioxidant? Insights from quantum chemistry calculations. *New J. Chem.* **46**, 162–168 (2022).
8. Straiker, A. et al. An evaluation of understudied phytocannabinoids and their effects in two neuronal models. *Molecules* **26**, 5352 (2021).
9. Hen-Shoval, D. et al. Acute oral cannabidiolic acid methyl ester reduces depression-like behavior in two genetic animal models of depression. *Behav. Brain Res.* **351**, 1–3 (2018).
10. Maccarrone, M. et al. Goods and bads of the endocannabinoid system as a therapeutic target: Lessons learned after 30 years. *Pharmacol. Rev.* **75**, 885–958 (2023).
11. Zhu, Y. F. et al. An evaluation of the anti-hyperalgesic effects of cannabidiolic acid-methyl ester in a preclinical model of peripheral neuropathic pain. *Br. J. Pharmacol.* **177**, 2712–2725 (2020).
12. Takeda, S. Cannabidiolic acid-mediated selective down-regulation of c-fos in highly aggressive breast cancer MDA-MB-231 cells: Possible involvement of its down-regulation in the abrogation of aggressiveness. *J. Nat. Med.* **71**, 286–291 (2017).
13. Serventi, L. et al. Comparative investigation of antimicrobial and antioxidant effects of the extracts from the inflorescences and leaves of the *Cannabis sativa* L. cv. strawberry. *Antioxidants* **12**, 219 (2023).
14. Appendino, G. et al. Antibacterial cannabinoids from *Cannabis sativa*: A structure-activity study. *J. Nat. Prod.* **71**, 1427–1430 (2008).
15. Stasiłowicz-Krzemień, A., Sip, S., Szulc, P., Walkowiak, J. & Cielecka-Piontek, J. The antioxidant and neuroprotective potential of leaves and inflorescences extracts of selected hemp varieties obtained with $scCO_2$. *Antioxidants* **12**, 1827 (2023).
16. Okimoto, T. et al. Antimicrobial-resistant *Helicobacter pylori* in Japan: Report of nationwide surveillance for 2018–2020. *Helicobacter* **29**, e13028 (2024).
17. Zheng, H., Xia, P., Fu, W. & Ding, S. *Helicobacter pylori* infection and inflammasomes. *Helicobacter* **29**, e13043 (2024).
18. Ashraf, J. & Riaz, M. A. Biological potential of copper complexes: A review. *Turk. J. Chem.* **46**, 595–623 (2022).
19. Kastal, Z. et al. Copper(II), nickel(II) and zinc(II) complexes of peptide fragments of tau protein. *Molecules* **29**, 2171 (2024).
20. Maret, W. Zinc biochemistry: From a single zinc enzyme to a key element of life. *Adv. Nutr.* **4**, 82–91 (2013).
21. Pezacki, A. T. et al. Oxidation state-specific fluorescent copper sensors reveal oncogene-driven redox changes that regulate labile copper(II) pools. *PNAS* **119**, e2202736119 (2022).
22. Kajornklin, P. Fabricating a low-cost, simple, screen printed paper towel-based experimental device to demonstrate the factors affecting chemical equilibrium and chemical equilibrium constant, K_c. *J. Chem. Educ.* **97**, 1984–1991 (2020).
23. Woźniczka, M. & Świątek, M. Transition metal complexes of reduced Schiff base and hydroxamic acid in aqueous systems: chemical equilibria and biological significance. In *Synthesis and Applications in Chemistry and Materials* (eds Pombeiro, A. J. L. et al.) 107–141 (World Scientific, 2024).
24. Gans, P. & O'Sullivan, B. GLEE, a new computer program for glass electrode calibration. *Talanta* **51**, 33–37 (2000).
25. Irving, H., Miles, M. G. & Pettit, L. D. A study of some problems in determining the stoicheiometric proton dissociation constants of complexes by potentiometric titrations using a glass electrode. *Anal. Chim. Acta* **38**, 475–488 (1967).
26. Mukherjee, G. & Chatterjee, S. Metal complexes of peptide derivatives. Part-XII. Mixed ligand complex formation of copper(II) with salicyloylglycylglycine and some typical N-donor ligands. *J. Indian Chem. Soc.* **75**, 341–344 (1998).
27. Mukherjee, G. N. & Ghosh, T. Mixed-ligand complex formation of cobalt(II), nickel(II) and zinc(II) with N-benzenesulphonyl-l-cysteine as primary ligand and bipyridine, ethylenediamine and glycinate as secondary ligands. *J. Indian Chem. Soc.* **74**, 8–11 (1997).
28. Gans, P., Sabatini, A. & Vacca, A. Investigation of equilibria in solution. Determination of equilibrium constants with the Hyperquad suite of programs. *Talanta* **43**, 1739–1753 (1996).
29. Woźniczka, M. et al. The complexing properties of oxalodihydrazide, acethydrazide and formic hydrazide with Cu(II) in aqueous solution. *Inorg. Chim. Acta* **455**, 659–665 (2017).

30. Alderighi, L. et al. Hyperquad simulation and speciation (HySS): A utility program for the investigation of equilibria involving soluble and partially soluble species. *Coordin. Chem. Rev.* **184**, 311–318 (1999).
31. Kostiainen, R. & Kauppila, T. J. Effect of eluent on the ionization process in liquid chromatography–mass spectrometry. *J. Chromatogr. A* **1216**, 685–699 (2009).
32. Brzeziński, M. et al. Nanocarriers based on block copolymers of l-proline and lactide: The effect of core crosslinking versus its pH-sensitivity on their cellular uptake. *Eur. Polym. J.* **156**, 110572 (2021).
33. Gonciarz, W., Chmiela, M., Kost, B., Piątczak, E. & Brzeziński, M. Stereocomplexed microparticles loaded with *Salvia cadmica* Boiss. extracts for enhancement of immune response towards *Helicobacter pylori*. *Sci. Rep.* **13**, 7039 (2023).
34. Gonciarz, W. et al. The effect of *Helicobacter pylori* infection and different *H. pylori* components on the proliferation and apoptosis of gastric epithelial cells and fibroblasts. *PLoSOne.* **14**, e0220636 (2019).
35. Gonciarz, W., Piątczak, E., Płoszaj, P., Gościniak, G. & Chmiela, M. *Salvia cadmica* extracts rich in polyphenols neutralize harmful effects of oxidative stress driven by *Helicobacter pylori* lipopolysaccharide in cell cultures of gastric epithelial cells or fibroblasts. *Ind. Crops Prod.* **178**, 114633 (2022).
36. Woźniczka, M. et al. Equilibria in aqueous cobalt(II)—reduced Schiff base N-(2-hydroxybenzyl)alanine system: Chemical characterization, kinetic analysis, antimicrobial and cytotoxic properties. *Molecules* **25**, 3462 (2020).
37. Woźniczka, M., Vogt, A. & Kufelnicki, A. Equilibria in cobalt(II)–amino acid– imidazole system under oxygen-free conditions: Effect of side groups on mixed-ligand systems with selected L-α-amino acids. *Chem. Cent. J.* **10**, 14 (2016).
38. Ramanaiah, M., Gouthamsri, S., Balakrishna, M., Ramaraju, B. & Rao, G. N. Effect of anionic micelles of sodium dodecyl sulfate on protonation equilibria of salicylic acid derivatives. *Cogent Chem.* **2**, 1217762 (2016).
39. Ke, J. et al. Determination of pKa values of alendronate sodium in aqueous solution by piecewise linear regression based on acid-base potentiometric titration. *J. Pharm. Anal.* **6**, 404–409 (2016).
40. Tomoaia-Cotisel, M. et al. Acid dissociation constants of diphytanylglycerolphosphorylglycerol-methylphosphate, and diphytanylglycerolphosphorylglycerophosphate and its deoxy analog. *Chem. Phys. Lipids* **100**, 41–54 (1999).
41. İnci, D. & Aydın, R. Structures, hydrolysis, stabilities of palladium(II) complexes containing biologically active ligands and species distribution in aqueous solution. *J. Mol. Struct.* **1187**, 23–37 (2019).
42. Wagner, M. R. & Walker, F. A. Spectroscopic study of 1:1 copper(II) complexes with Schiff base ligands derived from salicylaldehyde and L-histidine and its analogs. *Inorg. Chem.* **22**(21), 3021–3028 (1983).
43. Hinz, B. & Ramer, R. Cannabinoids as anticancer drugs: Current status of preclinical research. *Br. J. Cancer* **127**, 1–13 (2022).
44. Bęben, D. et al. Phytocannabinoids CBD, CBG, and their derivatives CBD-HQ and CBG-A induced in vitro cytotoxicity in 2D and 3D colon cancer cell models. *Curr. Issues. Mol. Biol.* **46**, 3626–3639 (2024).
45. Velasco, G., Sánchez, C. & Guzmán, M. Anticancer mechanisms of cannabinoids. *Curr. Oncol.* **23**(s1), 23–32 (2016).
46. McAllister, S. D. et al. Pathways mediating the effects of cannabidiol on the reduction of breast cancer cell proliferation, invasion, and metastasis. *Breast Cancer Res. Treat.* **129**, 37–47 (2011). Erratum in: *Breast Cancer Res. Treat.* **133**, 401–4 (2012).
47. Caffarel, M. M., Sarri´o, D., Palacios, J., Guzm´an, M. & S´anchez, C. Δ9- tetrahydrocannabinol inhibits cell cycle progression in human breast cancer cells through Cdc2 regulation. *Cancer Res.* **66**, 6615–6621 (2006).
48. Chmiela, M., Karwowska, Z., Gonciarz, W., Allushi, B. & Stączek, P. Host pathogen interactions in *Helicobacter pylori* related gastric cancer. *World J. Gastroenterol.* **23**, 1521–1540 (2017).
49. Papagiannakis, P., Michalopoulos, C., Papalexi, F., Dalampoura, D. & Diamantidis, M. D. The role of *Helicobacter pylori* infection in hematological disorders. *Eur. J. Intern. Med.* **24**, 685–690. https://doi.org/10.1016/j.ejim.2013.02.011 (2013).
50. Gonciarz, W. et al. Upregulation of MUC5AC production and deposition of LEWIS determinants by *HELICOBACTER PYLORI* facilitate gastric tissue colonization and the maintenance of infection. *J. Biomed. Sci.* **26**, 23 (2019).
51. Savoldi, A., Carrara, E., Graham, D. Y., Conti, M. & Tacconelli, E. Prevalence of antibiotic resistance in *Helicobacter pylori*: A systematic review and meta-analysis in world health organization regions. *Gastroenterology* **155**, 1372-1382.e17 (2018).
52. Martinenghi, L. D., Jønsson, R., Lund, T. & Jenssen, H. Isolation, purification, and antimicrobial characterization of cannabidiolic acid and cannabidiol from *Cannabis sativa* L. *Biomolecules* **10**, 900 (2020).
53. Kang, D. M. et al. Anti-*Helicobacter pylori* activity of six major compounds isolated from *Rumex acetosa*. *ACS Omega* **31**, 42548–42554 (2023).
54. Li, Y., Guo, S., Zou, H. & Chen, Y. Structure difference of Jack bean urease and *Helicobacter pylori* urease on binding interactions with quercetin. *Int. J. Biol. Macromol.* **307**, 141705 (2025).
55. Razmara, Z., Delarami, H. S., Eigner, V. & Dusek, M. Single crystal structure feature and quantum mechanical studies of a new binuclear Bi(III) complex and its activity against *Helicobacter pylori*. *Inorg. Chem. Commun.* **146**, 110207 (2022).
56. Huang, Y. et al. Curb challenges of the "Trojan Horse" approach: Smart strategies in achieving effective yet safe cell-penetrating peptide-based drug delivery. *Adv. Drug. Deliv. Rev.* **65**, 1299–1315 (2013).
57. Sutradhar, M. et al. A new Cu(II)-*O*-Carvacrotinate complex: Synthesis, characterization and biological activity. *J. Inorg. Biochem.* **190**, 31–37 (2019).

Acknowledgements

This work was supported by the Medical University of Lodz (Statute Fund No. 503/3-014-02/503-31-001 – M. Świątek; Statute Fund No. 503/3-066-02/503-31-001 – E. Budzisz) and the National Science Center with the grant SONATA 18 "Assessment of the ability of Mycobacterium bovis BCG-onco bacilli to control the development of Helicobacter pylori infection," UMO-2022/47/D/NZ7/01097. MLP and MC. We want to thank Professor Grazyna Gośniak (Department of Medical Microbiology, Wroclaw Medical University, Borowska 211a, 50-368 Wroclaw, Poland) for providing clinical strains of H. pylori for research.

Author contributions

M.W., W.G. designed the study. M.W., M.P., M.S., B.P., A.J.C., W.G. interpreted the data M.W., M.Ś., B.P., E.N., W.G. analyzed data. M.Ś. verified the data. M.W., W.G. wrote the original manuscript draf. M.W., M.P., M.S., M.Ś., B.P, A.J.C., E.N., W.G.: edited the final manuscript. All authors have read and approved the final manuscript.

Declarations

Competing interests

The authors declare no competing interests.

Additional information

Supplementary Information The online version contains supplementary material available at https://doi.org/1

0.1038/s41598-025-03442-5.

Correspondence and requests for materials should be addressed to M.W. or W.G.